JOURNAL OF CHEMICAL INFORMATION AND MODELING

Article

pubs.acs.org/jcim

Molecular Principle of Topotecan Resistance by Topoisomerase I Mutations through Molecular Modeling Approaches

Peichen Pan,[†] Youyong Li,[†] Huidong Yu,[†] Huiyong Sun,[†] and Tingjun Hou[†,‡,*]

[†]Institute of Functional Nano & Soft Materials (FUNSOM) and Jiangsu Key Laboratory for Carbon-Based Functional Materials & Devices, Soochow University, Suzhou, Jiangsu 215123, China

[‡]College of Pharmaceutical Sciences, Zhejiang University, Hangzhou, Zhejiang 310058, China

Supporting Information

ABSTRACT: Originally isolated from natural products, camptothecin (CPT) has provided extensive playing fields for the development of antitumor drugs. Two of the most successful analogs of CPT, topotecan and irinotecan, have been approved by the FDA for the treatment of colon cancer and ovarian cancer, as well as other cancers. However, the emergence of drug resistance mutations in topoisomerase I is a big challenge for the effective therapy of these drugs. Therefore, in this study, a series of computational approaches from molecular dynamics (MD) simulations to steered molecular dynamics (SMD) simulations and Molecular Mechanics/Generalized Born Surface Area (MM/GBSA) binding free energy calculations were employed to uncover the molecular principle of the topotecan resistance induced by three mutations in DNA topoisomerase I, including E418K, G503S, and D533G. Our results demonstrate a remarkable correlation between the binding free energies predicted by MM/GBSA and the rupture forces computed by SMD, and moreover, the theoretical results given by MM/GBSA and SMD are in excellent agreement with the experimental data for ranking the inhibitory activities: WT > E418K > G503S > D533G. In order to explore the drug resistance mechanism that underlies the loss of the binding affinity of topotecan, the binding modes of topotecan bound to the WT and mutated receptors were presented, and comparisons of the binding geometries and energy contributions on a per residue basis of topotecan between the WT complex and each mutant were also discussed. The results illustrate that the mutations of E418K, G503S, and D533G have great influence on the binding of topotecan to topoisomerase I bound with DNA, and the variations of the polar interactions play critical roles in the development of drug resistance. The information obtained from this study provides useful clues for designing improved topoisomerase I inhibitors for combating drug resistance.

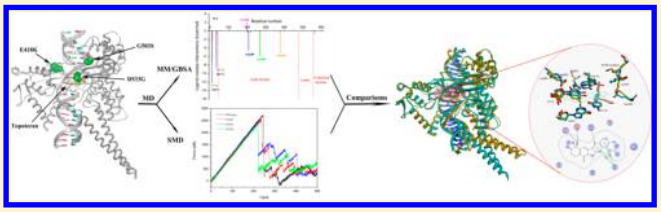

INTRODUCTION

Camptothecin (CPT) is a plant alkaloid isolated from the bark of a Chinese tree, *Camptotheca acuminata*, which has been widely used in traditional Chinese medicine (TCM). As a natural product, CPT was determined to be a potent anticancer agent in 1966 by Wall and co-workers.[1] However, the clinical trials of CPT were abandoned shortly thereafter due to its severe toxicity.[2−4] In the 1980s, human DNA topoisomerase I was identified as the only target for CPT, and this finding attracted great interest in the studies of CPT.[5−8] Numerous CPT analogs with acceptable solubility and satisfactory biological activities have been developed, and especially, two CPT analogs, topotecan and irinotecan, have been approved by the FDA for the treatment of ovarian cancer, cervical cancer, small cell lung cancer, and colon cancer.[9−12] In addition, lurtotecan, prothecan, exatecan, and belotecan have also been pushed into clinical trials for fighting a variety of cancers.[13−16]

Human DNA topoisomerase I is comprised of 765 residues, and it includes four main domains: C-terminal domain (residues from 713 to 765), N-terminal domain (residues from 1 to 214), core domain (residues from 215 to 635), and linker domain (residues from 636 to 712). The core domain of topoisomerase I can contact with DNA duplex and form a clamp surrounding the DNA. This segment is known as the "lips" region.[17] DNA topoisomerase I mediates the relaxation of DNA supercoils generated during transcription and replication by introducing a transient nick in one strand of duplex DNA. This process is involved in a nucleophilic attack by the hydroxyl group of Tyr723 on a DNA phosphodiester bond, forming a covalent 3′-phosphotyrosine binary enzyme−DNA complex. The 3′-phosphotyrosine linkage is then reattacked by the free 5′-hydroxyl group on the nicked DNA strand through a second tansesterification reaction, and the intact double-stranded DNA is released.[18] The inhibitors of DNA topoisomerase I, such as CPTs, have been shown to stabilize the 3′-phosphotyrosyl intermediate and inhibit the relegation step of the DNA phosphodiester backbone and enzyme release.

Great progress has been made in the development of CPT drugs, but a number of mutations have recently been identified in several regions of human DNA topoisomerase I to confer resistance to CPTs in vitro, in cultured cells, and in

Received: January 29, 2013
Published: March 22, 2013

dx.doi.org/10.1021/ci400066x | J. Chem. Inf. Model. 2013, 53, 997−1006

patients.[19−23] For example, the mutations of six residues, including Phe361,[19,24] Gly363,[19,25] Arg364,[22,23] Glu418,[26] Gly503,[20,27,28] and Asp533,[29,30] located in the lips region, usually lead to the resistance to CPT. Apart from the mutations in the lips region, the mutations of residues in the C-terminal domain (in particular Asn722 and Thr729) and Ala653 in the linker domain were also found to impair the binding of CPTs.[31−35] Because CPT is an uncompetitive inhibitor that only binds to the transient covalent 3′-phosphotyrosine binary enzyme−DNA complex, the binding modes and resistance mechanisms of CPT or CPT analogs are difficult to be studied by experiments. In 1998, the first X-ray crystal structure of human topoisomerase I covalently linked to a double-stranded DNA was reported.[36] In the following years, numerous crystal structures of topoisomerase I joined to double-stranded DNA and bound to CPT analogs were also available.[37] These structures afford the molecular basis for understanding the binding modes of CPT and CPT analogs, but they cannot explain the mechanisms of drug resistance induced by resistance mutations, especially mutations of the residues without forming direct protein-to-drug contacts. In 2004, the crystal structures of the Phe361Ser and Asn722Ser mutated human topoisomerase I in ternary complex with topotecan and DNA were reported by Chrencik and co-workers, and they provide valuable information to understand the resistance mechanisms of these two mutations.[38] However, the molecular mechanisms of drug resistance for the remaining mutations are not yet completely understood.

Molecular dynamics (MD) simulations have been successfully applied to investigate the influence of several resistance mutations on the dynamic features of DNA topoisomerase I and jointed DNA.[19,39] Benedetti et al. reported the MD simulations for the Ala653Pro mutant and presented that this mutation influences the flexibility of the linker domain.[40] In 2008, by using the MD simulations, Chillemi et al. observed that the mutations of Thr729 regulate the drug resistance by altering the protein communications between the C-terminal domain and the linker domain.[39] However, these simulations only qualitatively revealed the influence of some mutations on the dynamic properties of these mutants, and quantitative information, taking deep insights into the variation of each residue caused by resistance mutations, was still not provided. Therefore, in this study, a series of computational simulations, including MD simulations, Molecular Mechanics/Generalized Born Surface Area (MM/GBSA) free energy calculations, steered molecular dynamics (SMD) simulations, and MM/GBSA binding free energy decomposition, were employed to unveil the molecular principle of the topotecan resistance caused by three representative DNA topoisomerase I mutations in the lips region, including E418K, G503S, and D533G (Figure 1).[26−30] For the three studied mutations, the resistance mechanisms to CPT or CPT analogs still remain a mystery.

MATERIALS AND METHODS

1. Initial Structures. The crystallographic structure of the human wild-type (WT) DNA topoisomerase I linked to a double-stranded DNA and bound to topotecan (PDB entry, 1K4T; resolution, 2.10 Å) was retrieved from the RCSB Brookhaven Protein Data Bank.[37,41] Because the X-ray crystal structures of the studied mutants are not available, these structures were generated by mutating their corresponding amino acids in the WT structure with the Discovery Studio 2.5 package.[42] In the WT crystal structure, only the core domain, C-terminal domain and linker domain are contained, and the N-terminal domain has not been resolved. However, the residues in the active site are included in the core domain of the structure. The three constructed models for the mutants and the WT crystal structure of the topoisomerase I/DNA/topotecan ternary complex were applied as the initial structures for the following simulations.

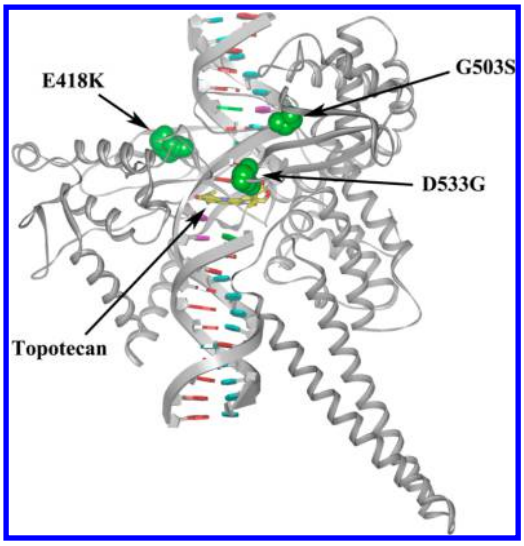

Figure 1. Ribbon schematic representation of topoisomerase I bound with DNA and topotecan. The positions of the three studied mutations (E418K, G503S, and D533G) are highlighted.

After optimization, topotecan was optimized at HF/6-31G* level of theory using the Gaussian 09 program.[43] Subsequently, the atomic partial charges were obtained by a restraint electrostatic potential fit method.[40] The partial charges and missing force-field parameters for topotecan were generated by the *antechamber* suite.[44] The general AMBER force field (*gaff*)[45] and the Amber99SB force field[46] were used for topotecan and receptor, respectively. All missing atoms in the receptor were added using the *leap* program,[44] and 19 counterions of Na^+ were placed into the system to neutralize the negative charge of each system. Then, each system was immersed into a periodic TIP3P water box that was extended 12 Å from any solute atom. The Particle Mesh Ewald (PME) algorithm was used to handle the long-range electrostatics.[47]

2. Molecular Dynamics (MD) Simulations. The MD simulations were carried out using the Amber11 molecular simulation package.[44] The four systems were first subjected to a three-stage minimization by the *sander* program.[44] First, 1000 cycles of minimization (500 cycles of steepest descent and 500 cycles of conjugate gradient) were carried out with protein backbone and DNA heavy atoms constrained (50 kcal/mol/Å^2). Second, another minimization stage with a relatively weaker constrain (10 kcal/mol/Å^2) was conducted. Then, each complex was submitted to 5000 cycles of energy minimization without any constrain (1000 cycles of steepest descent and 4000 cycles of conjugate gradient). Subsequently, each system was gradually heated from 0 to 300 K over a period of 50 ps with 2.0 kcal/mol/Å^2 restrain on the complex, and then another 50 ps MD simulations were followed at 300 K with the same restrain. Afterward, for each system, 30 ns NPT MD simulations with the target temperature of 300 K and target pressure of 1 atm were performed to produce trajectories. However, for the G503S mutant, extra 30 ns MD simulations

were carried out for stabilizing the whole system. All bonds involving hydrogen atoms were constrained with the SHAKE algorithm,[46] and the time step was set to 2.0 fs.

3. Steered Molecular Dynamics (SMD) Simulations. The SMD simulations were implemented by the NAMD software using the last snapshot of each MD simulations.[48] The preparations of the structures for the SMD simulations were accomplished with the same procedures as we have described in the Initial Structures section. The total box size of the WT system is about 97.9 Å × 123.7 Å × 106.4 Å that contains roughly 35,600 water molecules, and the center of the complex was placed at the position of 50.4, 63.3, and 55.1 Å. According to the complex structures, only one pulling path (Figure S1, Supporting Information) with the largest pocket size and fewest obstacles in the pulling tunnel for topotecan was determined by Caver 2.0, a plugin of PyMOL.[49] This pulling direction goes through the tunnel encircled by the residues Glu267, Arg362, Arg364, Ile535, His632, Gln633, Ala635, and DA13. The pulling path of each complex was directed along the z-direction. First, we performed 40 ps MD equilibration in the absence of pulling force with the backbone constrained (5 kcal/mol/Å^2). Then, 500 ps SMD simulations were carried out to pull topotecan from the binding pocket along the z-direction by applying a force on the C11 atom of topotecan . The total force was predicted by the equation $F = k(vt - x)$, where k, that was set to 3.0 kcal/mol/Å^2 in our simulations, is the cantilever spring constant, v represents the pulling velocity that we set to 0.00012 Å/time step (1time step = 2 fs), and x stands for the shifting of the pulled atom from its initial position.

4. MM/GBSA Free Energy Calculations. The fast and accurate MM/GBSA methodology, which combines molecular mechanics and continuum solvent model, was utilized to calculate the binding free energy for the four systems.[50−68] The MM/GBSA binding free energy was predicted based on eq 1. In our calculations, the single-trajectory protocol with higher stability of prediction was employed.

$$\begin{aligned}\Delta G_{\text{bind}} &= G_{\text{complex}} - G_{\text{protein}} - G_{\text{ligand}} \\ &= \Delta H + \Delta G_{\text{solvation}} - T\Delta S \\ &= \Delta E_{\text{MM}} + \Delta G_{\text{GB}} + \Delta G_{\text{SA}} - T\Delta S \end{aligned} \quad (1)$$

where ΔE_{MM} represents the gas-phase interaction energy between ligand and receptor, which contains the electrostatic and van der Waals contributions; ΔG_{GB} and ΔG_{SA} stand for the polar and nonpolar components of the desolvation free energy; and $-T\Delta S$ is the change of the conformational entropy. The entropic contributions were computed for the four systems using the *nmode* program in Amber.[44] Because of a highly computational cost, we only considered the residues within a 10 Å sphere centered at the ligand.[64] The generalized Born (GB) model with the parameter developed by Onufriev and co-workers (*igb* = 2) was used to calculate the polar contribution of desolvation (ΔG_{GB}).[69] The nonpolar contribution of the desolvation free energy (ΔG_{SA}) was predicted by the solvent-accessible surface area (SASA) on the basis of the LCPO method: ΔG_{SA}= 0.0072 × ΔSASA.[70] The solute dielectric constant was set to 1, and the exterior dielectric constant was set to 80. The calculations of the energy terms were based on 100 snapshots extracted evenly from the last stable 10 ns trajectories of each system.

5. Binding Free Energy Decomposition Analysis. In order to investigate the contribution and variation of each residue on the topotecan binding, the MM/GBSA binding free energy decomposition supported by the *mm_pbsa* program of Amber11 was executed on a per-residue basis.[63,67] As displayed in eq 2, four components are included in the interactions between ligand and each residue.

$$\Delta G_{\text{inhibitor−residue}} = \Delta E_{\text{vdw}} + \Delta G_{\text{ele}} + \Delta G_{\text{GB}} + \Delta G_{\text{SA}} \quad (2)$$

where ΔE_{vdw} and ΔE_{ele} stand for the van der Waals and electrostatic contributions, and ΔG_{GB} and ΔG_{SA} represent the polar and nonpolar desolvation contributions, respectively. The GB model (*igb* = 2) was used to calculate the polar contribution of desolvation (ΔG_{GB}).[69] The nonpolar contribution of the desolvation free energy (ΔG_{SA}) was computed by the SASA based on the ICOSA technique.[67] The solute dielectric constant and the exterior dielectric constant were set to 1 and 80, respectively.

RESULTS AND DISCUSSION

1. Structural Stability and Flexibility of the WT and Mutated Complexes. The root-mean-square displacement (RMSD) of each system is illustrated in Figure S2 of the Supporting Information. It can be observed that the WT complex achieves equilibrium much earlier than the mutants. This is not surprising because the alteration of the mutation site would change the properties of the corresponding residues and might introduce perturbation to the original structure. The RMSDs of the residues within 5 Å of topotecan were also calculated and plotted in Figure 2. We can observe that the residues surrounding the binding pocket for all systems reach stability much earlier. Moreover, it is interesting to find that the RMSDs of the active site residues for the G503S mutant are not quite stable until 20 ns. This may indicate that the G503S mutation leads to relatively larger conformational changes for the binding of topotecan to the topoisomerase I/DNA complex due to its outlying location away from the drug. In order to evaluate the stability of each residue, the root-mean-square fluctuation (RMSF) based on the last 10 ns trajectory of each system is plotted in Figure 3. According to the comparison of the RMSFs, little difference is observed between the WT and each mutant. The core domain, C-terminal domain, and DNA duplex are more stable than the linker domain. The structures of the linker domain in all four systems keep swinging during the whole simulations, exhibiting a flexible behavior.

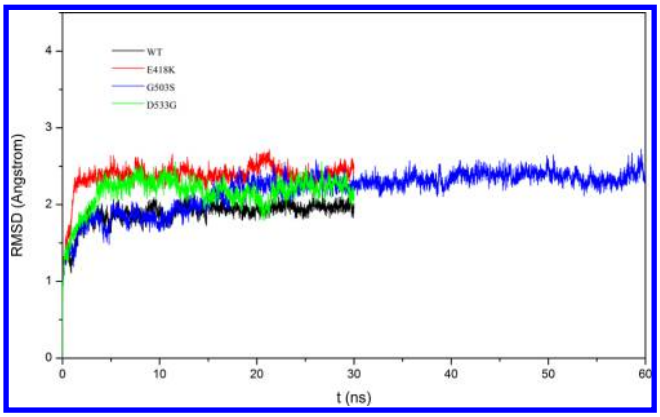

Figure 2. Illustration of the root-mean-square displacements (RMSDs) of the residues within 5 Å of topotecan of each system (black, WT; red, E418K; blue, G503S; green, D533G).

dx.doi.org/10.1021/ci400066x | J. Chem. Inf. Model. 2013, 53, 997−1006

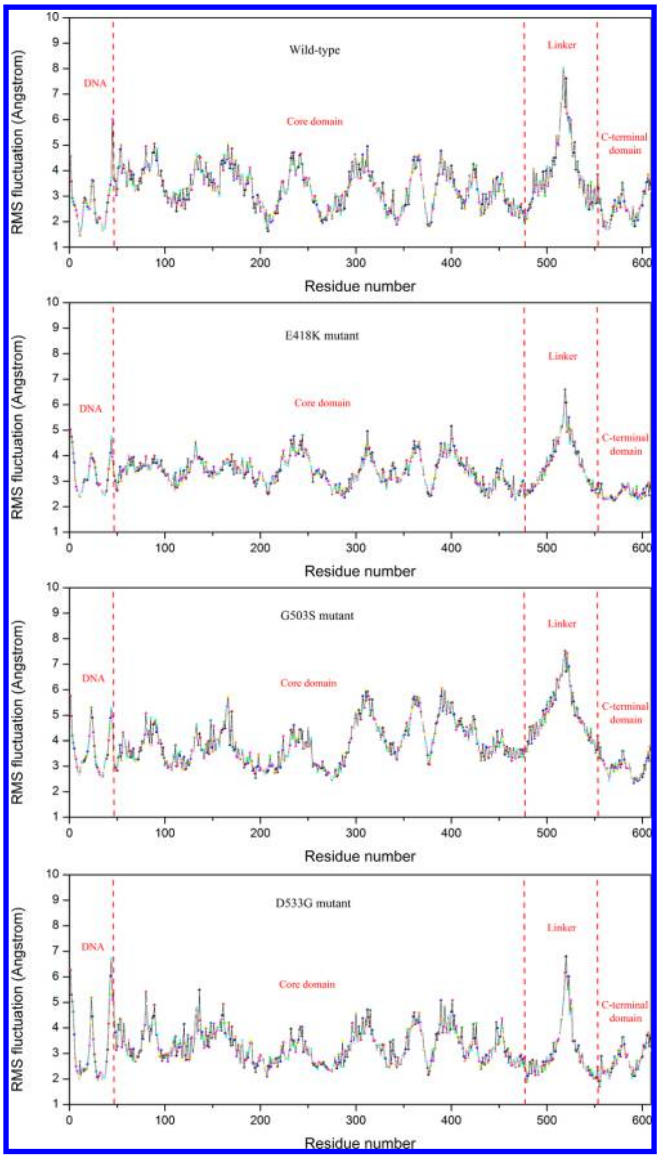

Figure 3. Schematic representation of the root-mean-square fluctuations (RMSFs) based on the last 10 ns MD trajectories of the WT complex and the three studied mutants.

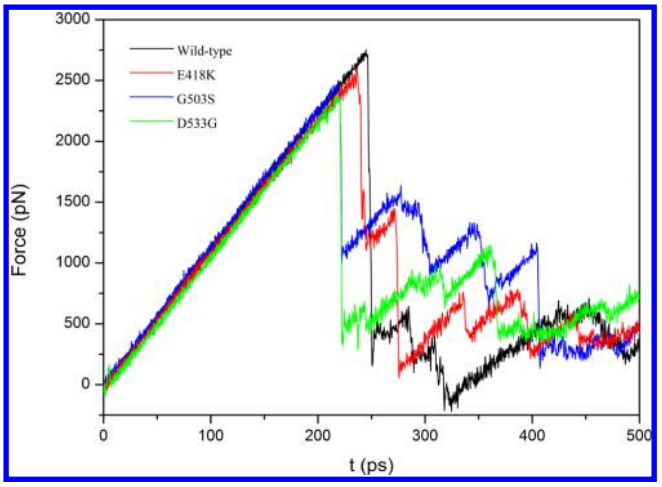

Figure 4. Force-time profiles of topoisomerase I bound with DNA and topotecan, obtained by pulling tooptecan from the WT complex and the E418K, G503S, and D533G mutants (black, WT; red, E418K; blue, G503S; green, D533G). The external force is set along the z-direction.

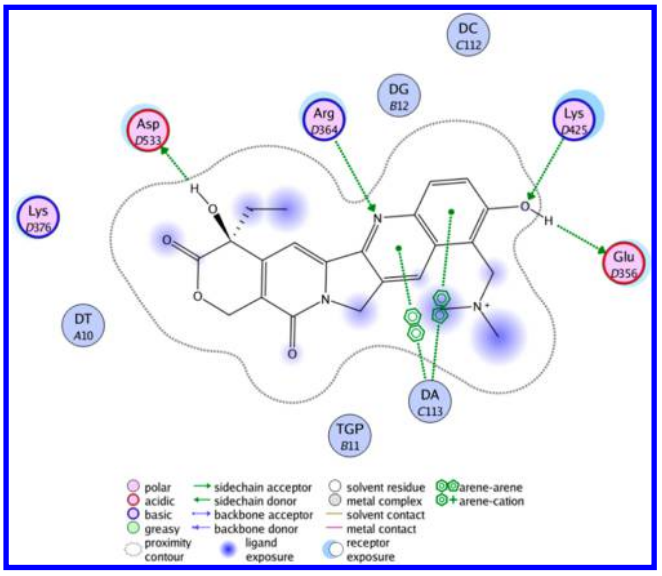

Figure 5. Schematic representation of the interactions between topotecan and the WT topoisomerase I bound with DNA.

2. Assessment of Drug Resistance by MM/GBSA Calculations and SMD Simulations. The binding affinities (ΔG_{bind}) and the energy components predicted by MM/GBSA for the WT complex and three mutants are summarized in Table 1 based on the last 10 ns trajectories. The predicted binding free energies of the E418K, G503S, and D533G mutants by MM/GBSA are −53.13, −52.82, and −41.79 kcal/mol, respectively, which are all higher than that of the WT system (−56.90 kcal/mol). This indicates that the binding affinities of topotecan to three mutants are reduced. Moreover, we can observe that the rank of the binding affinities for all systems are correctly predicted by the ΔG_{bind} values, which is

Table 1. Energy Components of Predicted Binding Free Energies between Topotecan and Topoisomerase I/DNA Complex (ε_{in} = 1.0)[a]

energy	wild-type	E418K	G503S	D533G
ΔE_{vdw}	−64.70 ± 0.50	−64.32 ± 1.10	−63.74 ± 0.46	−61.97 ± 0.92
ΔG_{SA}	−3.64 ± 0.04	−3.60 ± 0.02	−3.37 ± 0.01	−3.24 ± 0.03
ΔE_{ele}	−54.12 ± 1.38	−45.29 ± 3.07	−40.01 ± 5.64	−26.29 ± 0.26
ΔG_{GB}	65.54 ± 1.41	60.07 ± 1.07	54.27 ± 4.65	49.69 ± 0.09
ΔG_{total}	−56.90 ± 0.49	−53.13 ± 0.89	−52.82 ± 0.54	−41.79 ± 0.55
cellular resistance	–	15-fold	134-fold	300-fold

[a]Standard deviations based on two blocks.

dx.doi.org/10.1021/ci400066x | J. Chem. Inf. Model. 2013, 53, 997−1006

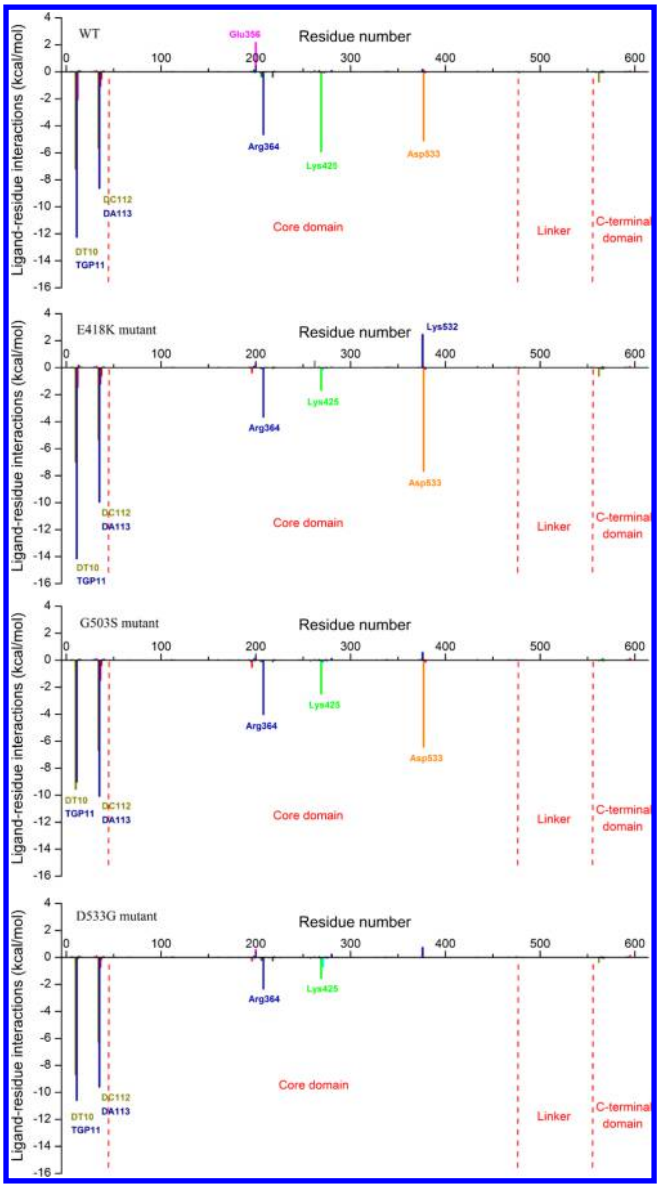

Figure 6. Residue−drug interaction spectra of the WT complex and the three studied mutants.

well consistent with the experimental data.[26−30] The calculated $T\Delta S$ for WT, E418K, G503S, and D533G are −15.53, −14.03, −13.75, and −13.90 kcal/mol, respectively. When $T\Delta S$ is considered, the binding free energies for WT, E418K, G503S, and D533G are −41.37, −39.10, −39.07, and −27.89 kcal/mol, respectively. It can be observed that the rank of the binding affinities for the four systems are also correct, but the difference between E418K and G503S is not so obvious. It is not surprising because the previous studies show that the inclusion of the conformational entropy does not always improve the prediction accuracy.[64] MM/GBSA or MM/PBSA can still achieve ideal accuracy of ranking ligand affinities without considering conformational entropy.

It was recently reported that SMD can be a promising tool to predict the binding affinities for ligand−protein systems.[71−73] For example, in 2011, Binh et al. reported a high correlation (r = 0.97) between the rupture forces (F_{max}) estimated from SMD and the experimental binding energies for R-125489 and CS-8958 to neuraminidases (NAs) of influenza virus. According to their studies, SMD gives similar performance to the molecular mechanics/Poisson−Boltzmann surface area (MM/PBSA) method.[71] In this study, the SMD simulations were employed and validated as a complementary tool for MM/GBSA. The typical force-time profiles for the four studied systems are shown in Figure 4. Mechanically, the binding affinity between topotecan and the WT complex is the strongest because the WT system has the highest force peak, and the rank-order of the rupture forces (F_{max}) for the other three mutants is also correct. Thus, the MM/GBSA calculations and the SMD simulations give a reasonable agreement with the experimental results and provide evidence for the accuracy of our predictions for drug resistance.

The binding free energy components for each system are also presented in Table 1. We can find that the van der Waals (ΔE_{vdw}), electrostatic (ΔE_{ele}), and nonpolar desolvation (ΔG_{SA}) terms are favorable to the topotecan binding, whereas the polar desolvation term (ΔG_{GB}) is unfavorable. The nonpolar energies (ΔE_{vdw} + ΔG_{SA}) of the WT, E418K, G503S, and D533G complexes are −68.34, −67.92, −67.11, and −65.21 kcal/mol, respectively. For the three mutants, the nonpolar interactions are slightly weakened but not much compared with that for the WT complex. Large differences are observed for the polar interactions, including the electrostatic (ΔE_{ele}) and polar desolvation terms (ΔG_{GB}). The polar energies (ΔE_{ele} + ΔG_{GB}) for the E418K, G503S, and D533G mutants are 14.78, 14.26, and 23.40 kcal/mol, respectively, which are all higher than that of the WT complex (11.42 kcal/mol). Our data suggest that the polar interactions play critical roles in determining the resistance capability of the E418K, G503S, and D533G mutations to topotecan.

3. Effect of Mutations on the Binding of Topotecan to Topoisomerase I/DNA Complex. To unveil the molecular principle of the topotecan resistance at the atomic level, the receptor drug interaction spectrum for each system on a per-residue basis was generated by the MM/GBSA free energy decomposition analysis, and the comparison of the binding geometries of topotecan between the WT complex and each mutant is also presented.

3.1. Binding Mode of topotecan to WT Complex. According to the energy decomposition analysis (Figure 6), the essential residues for the binding of topotecan to the WT complex are DT10, TGP11, DC112, DA113, Arg364, Lys425, and Asp533. The energy components of these important residues are also listed in Table S1 of the Supporting Information. We can observe that the nonpolar interactions of DT10, TGP11, DC112, and DA113 in the DNA duplex contribute strongly to binding, and the favorable polar interactions are primarily contributed from the residues Arg364, Lys425, and Asp533. As we see in Figure 5, topotecan forms strong $\pi-\pi$ stacking interactions with DA113 and four H-bonds with Asp533, Arg364, Lys425, and Glu356, which play critical roles in ligand binding. Despite of the strong electrostatic interactions with topotecan, the total polar contribution (ΔE_{ele} + ΔG_{GB}) of the residue Glu356 is positive due to the unfavorable polar desolvation energy.

3.2. Resistance Mechanism of E418K Mutation. To understand the influence of the E418K mutation on the binding of topotecan, the average structure generated from the last 10 ns MD trajectory of the E418K complex was superimposed on that of the WT complex. As shown in Figure 7a, the backbone structure of the E418K mutant is quite similar to that of the WT complex except for the linker domain with

dx.doi.org/10.1021/ci400066x | J. Chem. Inf. Model. 2013, 53, 997−1006

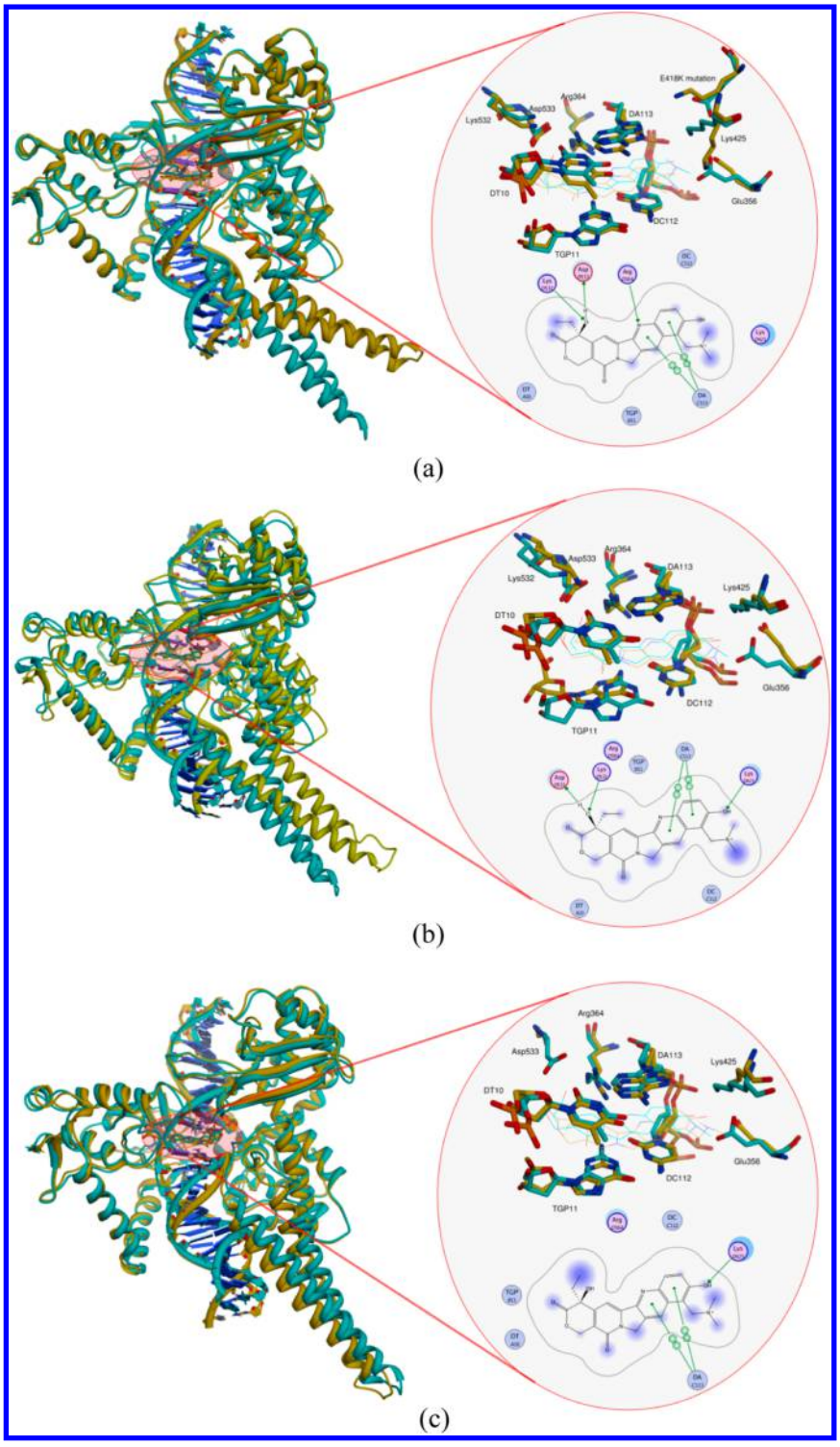

Figure 7. Structural superimposition of the WT (cyan) and (a) E418K (yellow), (b) G503S (yellow), or (c) D533G mutant (yellow) of topoisomerase I bound with DNA and topotecan. All structures are average conformations generated from the last 10 ns snapshots of each system. On the right-hand of the illustration, superimposition of the key residues in the binding pocket of the WT complex (cyan) with that of the mutant (yellow) and schematic representation of the interactions between topotecan and each mutant.

the tail cocked. Furthermore, a close-up view of the binding site reveals that most residues of these two systems are well aligned. However, the flexible residue, Lys425, has a huge conformational change, and the H-bond with topotecan that is found in the WT system disappears. This is consistent with the free energy decomposition results, where the contribution of Lys425 drops dramatically compared with that in the WT system. The site of the E418K mutation does not have a direct contact with topotecan, but an intraprotein H-bond in the WT complex between Glu418 and Lys425 can be observed. This H-bond functions as a bridge to connect the communication between Lys425 and the 10-hydroxy group of topotecan. Once Glu418 is mutated to lysine, the H-bond between residue 418 and Lys425 is disrupted, resulting in the significant conforma-

dx.doi.org/10.1021/ci400066x | J. Chem. Inf. Model. 2013, 53, 997−1006

tional change of Lys425 and affecting the H-bond between topotecan and Lys425. In addition to the influence of Lys425, the contribution of Arg364 is also slightly reduced, but the H-bond between topotecan and Arg364 is still maintained. The variations of the DNA duplex in the binding site are limited, exhibiting conservative behavior.

3.3. Resistance Mechanism of G503S Mutation. Glycine 503 is also a nonactive site residue, which cannot form direct contact with topotecan. However, the G503S mutation belongs to the substitution of a smaller glycine group with a larger serine group, so the addition of the hydroxymethyl group in serine may significantly affect the conformation of the protein/DNA complex due to the formation of the H-bonds between the mutated Ser503 and the surrounding amino acids (not shown), which cannot be observed in the WT complex. This conformational change indirectly results in the rearrangement of the binding site residues. According to the result of the MD simulations, it takes approximately 40 and 20 ns to stabilize the whole system and the binding site residues, respectively. The superimposition of the WT complex and the G503S mutant is illustrated in Figure 7b. We can find that most binding site residues of the G503S mutant do not have huge conformational change, but significant slide of the residue TGP11 is noticed. The binding free energy decomposition analysis (Figure 6) also demonstrates an obvious reduction of the energy contribution of the residue TGP11. Another conspicuous displacement is found in the residue Glu356, but the contribution of this residue in both the WT system and G503S mutant is negligible. Apart from the variation of TGP11, the contribution of the residue Lys425 is also substantially reduced. Different from the situation of the E418K mutant, the structure of Lys425 in the G503S mutant does not change obviously compared with that in the WT complex, and only the position of topotecan slightly changes. According to the energy decomposition results, the energy reduction of Lys425 mainly results from the impact of the polar interactions ($\Delta E_{ele} + \Delta G_{GB}$), which indicates that even subtle alteration of the ligand geometry can produce profound difference of the electrostatic interactions. Moreover, the H-bond between Arg364 and topotecan is not detected with the polar interactions weakened, but the total contribution of Arg364 is only slightly influenced due to the increase of the nonpolar contributions.

3.4. Resistance Mechanism of D533G Mutation. Asp533 is located in the lips region of the binding pocket and forms direct contact with topotecan in the WT complex. A strong H-bond between the carboxy oxygen of Asp533 and the hydroxy hydrogen of topotecan can be observed. The D533G mutation belongs to the replacement of a larger group with a smaller glycine group. It is easy to predict that most obvious influence would come from the removal of the carboxymethyl group, which directly responses for the missing of the interactions between the residue 533 and topotecan. According to our simulation results, the energy contribution of Gly533 almost falls to zero. The structural superimposition of the WT complex and the D533G mutant (Figure 7c) also reveals that no significant change of the geometry of the residues in the D533G mutant is found. However, topotecan is obviously shifted from the original position in the WT complex due to the loss of the strong interactions with the residue 533. This variation leads to the rearrangement of the energy distribution of the surrounding residues. Both the residue Arg364 and Lys425 are affected by the shift of topotecan and their energy contributions are significantly reduced. For the residues of DNA in the binding pocket, however, only the interactions of the residue TGP11 is weakened, and the energy contributions of the residues DT10, DC112, and DA113 are slightly increased. The total energies of the four residues to the topotecan binding in the WT complex and the D533G mutant are −35.16 and −33.74 kcal/mol, respectively, suggesting that the D533G mutation does not have strong effects on the interactions between topotecan and the DNA residues.

CONCLUSIONS

In this study, we used a series of molecular modeling techniques, including conventional MD simulations, MM/GBSA binding free energy predictions, SMD simulations, and MM/GBSA binding free energy decomposition analysis, to explore the impact of three resistance mutations in topoisomerase I on the topotecan binding. The predicted binding free energies of topotecan to the WT complex and the three studied mutants are consistent with the experimental data. According to the results of the SMD simulations, the rupture forces on behalf of the stability of the ligand−protein complexes are in good agreement with the binding free energies predicted by MM/GBSA. Results of both MM/GBSA calculations and SMD simulations give correct order to rank the inhibitory potency of the studied systems: WT > E418K > G503S > D533G.

Moreover, our computational simulations demonstrate that the mutations of E418K, G503S, and D533G have great influence on the binding of topotecan to topoisomerase I bound with DNA, and the variations of the polar interactions, primarily involving in the residues Arg364, Lys425, and Asp533, play critical roles in the development of drug resistance. The influence on the nonpolar interactions are limited because the strong and wide-ranging van deer Waals contributions of the DNA duplex are quite stable. The structural analysis from this work uncovers the obscure mechanisms of the topotecan resistance by both active and nonactive site mutations of topoisomerase I and provide a valuable clue for the design of improved inhibitors to combat resistance.

ASSOCIATED CONTENT

Supporting Information

Table S1: Contributions of the important residues for the binding of topotecan with the WT complex (kcal/mol). Figure S1: Ribbon schematic representation of the pulling z-direction of topotecan bound with the topoisomerase I/DNA complex for SMD simulations. Figure S2: Illustration of the root-mean-square displacements (RMSDs) of the WT complex and three studied mutants (black, WT; red, E418K; blue, G503S; green, D533G). This material is available free of charge via the Internet at http://pubs.acs.org.

AUTHOR INFORMATION

Corresponding Author

*E-mail: tingjunhou@hotmail.com. Phone: +86-512-65882039.

Notes

The authors declare no competing financial interest.

ACKNOWLEDGMENTS

This study was supported by the National Science Foundation of China (21173156), National Basic Research Program of China (973 program, 2012CB932600), and Priority Academic Program Development of Jiangsu Higher Education Institutions (PAPD).

REFERENCES

(1) Wall, M. E.; Wani, M.; Cook, C.; Palmer, K. H.; McPhail, A.; Sim, G. Plant antitumor agents. I. The isolation and structure of camptothecin, a novel alkaloidal leukemia and tumor inhibitor from camptotheca acuminata1, 2. *J. Am. Chem. Soc.* **1966**, *88*, 3888−3890.

(2) Moertel, C. G.; Schutt, A. J.; Reitemeier, R.; Hahn, R. Phase II study of camptothecin (NSC-100880) in the treatment of advanced gastrointestinal cancer. *Cancer Chemother. Rep., Part 1* **1972**, *56*, 95.

(3) Schaeppi, U.; Fleischman, R.; Cooney, D. Toxicity of camptothecin (NSC-100880). *Cancer Chemother. Rep., Part 3* **1974**, *5*, 25.

(4) Gottlieb, J. A.; Luce, J. K. Treatment of malignant melanoma with camptothecin (NSC-100880). *Cancer Chemother. Rep., Part 1* **1972**, *56*, 103.

(5) Hsiang, Y. H.; Hertzberg, R.; Hecht, S.; Liu, L. Camptothecin induces protein-linked DNA breaks via mammalian DNA topoisomerase I. *J. Biol. Chem.* **1985**, *260*, 14873−14878.

(6) Hsiang, Y. H.; Liu, L. F. Identification of mammalian DNA topoisomerase I as an intracellular target of the anticancer drug camptothecin. *Cancer Res.* **1988**, *48*, 1722−1726.

(7) Hsiang, Y. H.; Lihou, M. G.; Liu, L. F. Arrest of replication forks by drug-stabilized topoisomerase I-DNA cleavable complexes as a mechanism of cell killing by camptothecin. *Cancer Res.* **1989**, *49*, 5077−5082.

(8) Giovanella, B. C.; Stehlin, J. S.; Wall, M. E.; Wani, M. C.; Nicholas, A. W.; Liu, L. F.; Silber, R.; Potmesil, M. DNA topoisomerase I: Targeted chemotherapy of human colon cancer in xenografts. *Science* **1989**, *246*, 1046.

(9) ten Bokkel Huinink, W.; Gore, M.; Carmichael, J.; Gordon, A.; Malfetano, J.; Hudson, I.; Broom, C.; Scarabelli, C.; Davidson, N.; Spanczynski, M. Topotecan versus paclitaxel for the treatment of recurrent epithelial ovarian cancer. *J. Clin. Oncol.* **1997**, *15*, 2183−2193.

(10) Long, H. J., III; Bundy, B. N.; Grendys, E. C., Jr.; Benda, J. A.; McMeekin, D. S.; Sorosky, J.; Miller, D. S.; Eaton, L. A.; Fiorica, J. V. Randomized phase III trial of cisplatin with or without topotecan in carcinoma of the uterine cervix: a Gynecologic Oncology Group Study. *Journal of Clinical Oncology* **2005**, *23*, 4626−4633.

(11) O'Brien, M. E. R.; Ciuleanu, T. E.; Tsekov, H.; Shparyk, Y.; Čučeviá, B.; Juhasz, G.; Thatcher, N.; Ross, G. A.; Dane, G. C.; Crofts, T. Phase III trial comparing supportive care alone with supportive care with oral topotecan in patients with relapsed small-cell lung cancer. *J. Clin. Oncol.* **2006**, *24*, 5441−5447.

(12) Cunningham, D.; Pyrhönen, S.; James, R. D.; Punt, C. J. A.; Hickish, T. F.; Heikkila, R.; Johannesen, T. B.; Starkhammar, H.; Topham, C. A.; Awad, L. Randomised trial of irinotecan plus supportive care versus supportive care alone after fluorouracil failure for patients with metastatic colorectal cancer. *Lancet* **1998**, *352*, 1413−1418.

(13) Dark, G. G.; Calvert, A. H.; Grimshaw, R.; Poole, C.; Swenerton, K.; Kaye, S.; Coleman, R.; Jayson, G.; Le, T.; Ellard, S. Randomized trial of two intravenous schedules of the topoisomerase I inhibitor liposomal lurtotecan in women with relapsed epithelial ovarian cancer: A trial of the National Cancer Institute of Canada Clinical Trials Group. *J. Clin. Oncol.* **2005**, *23*, 1859−1866.

(14) Pasut, G.; Veronese, F. M. PEG conjugates in clinical development or use as anticancer agents: An overview. *Adv. Drug Delivery Rev.* **2009**, *61*, 1177−1188.

(15) Abou-Alfa, G. K.; Letourneau, R.; Harker, G.; Modiano, M.; Hurwitz, H.; Tchekmedyian, N. S.; Feit, K.; Ackerman, J.; De Jager, R. L.; Eckhardt, S. G. Randomized phase III study of exatecan and gemcitabine compared with gemcitabine alone in untreated advanced pancreatic cancer. *J. Clin. Oncol.* **2006**, *24*, 4441−4447.

(16) Lee, D.; Kim, S. W.; Suh, C.; Lee, J. S.; Lee, J.; Lee, S. J.; Ryoo, B.; Park, K.; Kim, J.; Heo, D. Belotecan, new camptothecin analogue, is active in patients with small-cell lung cancer: Results of a multicenter early phase II study. *Ann. Oncol.* **2008**, *19*, 123−127.

(17) Redinbo, M. R.; Stewart, L.; Kuhn, P.; Champoux, J. J.; Hol, W. G. J. Crystal structures of human topoisomerase I in covalent and noncovalent complexes with DNA. *Science* **1998**, *279*, 1504−1513.

(18) Wang, J. C. DNA topoisomerases. *Annu. Rev. Biochem.* **1996**, *65*, 635−692.

(19) Benedetti, P.; Fiorani, P.; Capuani, L.; Wang, J. C. Camptothecin resistance from a single mutation changing glycine 363 of human DNA topoisomerase I to cysteine. *Cancer Res.* **1993**, *53*, 4343−4348.

(20) Tanizawa, A.; Beitrand, R.; Kohlhagen, G.; Tabuchi, A.; Jenkins, J.; Pommier, Y. Cloning of Chinese hamster DNA topoisomerase I cDNA and identification of a single point mutation responsible for camptothecin resistance. *J. Biol. Chem.* **1993**, *268*, 25463−25468.

(21) Wang, L. F.; Ting, C. Y.; Lo, C. K.; Su, J. S.; Mickley, L. A.; Fojo, A. T.; Whang-Peng, J.; Hwang, J. Identification of mutations at DNA topoisomerase I responsible for camptothecin resistance. *Cancer Res.* **1997**, *57*, 1516−1522.

(22) Urasaki, Y.; Laco, G. S.; Pourquier, P.; Takebayashi, Y.; Kohlhagen, G.; Gioffre, C.; Zhang, H.; Chatterjee, D.; Pantazis, P.; Pommier, Y. Characterization of a novel topoisomerase I mutation from a camptothecin-resistant human prostate cancer cell line. *Cancer Res.* **2001**, *61*, 1964−1969.

(23) Li, X. G.; Paul, H., Jr.; Yaw-Huei, H.; Ajit, K. B.; Donald, W. K.; Leroy, F. L.; Eric, H. R. Involvement of amino acids 361 to 364 of human topoisomerase I in camptothecin resistance and enzyme catalysis. *Biochem. Pharmacol.* **1997**, *53*, 1019−1027.

(24) Rubin, E.; Pantazis, P.; Bharti, A.; Toppmeyer, D.; Giovanella, B.; Kufe, D. Identification of a mutant human topoisomerase I with intact catalytic activity and resistance to 9-nitro-camptothecin. *J. Biol. Chem.* **1994**, *269*, 2433−2439.

(25) Fiorani, P.; Amatruda, J. F.; Silvestri, A.; Butler, R. H.; Bjornsti, M. A.; Benedetti, P. Domain interactions affecting human DNA topoisomerase I catalysis and camptothecin sensitivity. *Mol. Pharmacol.* **1999**, *56*, 1105−1115.

(26) Chang, J. Y.; Liu, J. F.; Juang, S. H.; Liu, T. W.; Chen, L. T. Novel mutation of topoisomerase I in rendering cells resistant to camptothecin. *Cancer Res.* **2002**, *62*, 3716−3721.

(27) Tanizawa, A.; Pommier, Y. Topoisomerase I alteration in a camptothecin-resistant cell line derived from Chinese hamster DC3F cells in culture. *Cancer Res.* **1992**, *52*, 1848−1854.

(28) Urasaki, Y.; Laco, G.; Takebayashi, Y.; Bailly, C.; Kohlhagen, G.; Pommier, Y. Use of camptothecin-resistant mammalian cell lines to evaluate the role of topoisomerase I in the antiproliferative activity of the indolocarbazole, NB-506, and its topoisomerase I binding site. *Cancer Res.* **2001**, *61*, 504−508.

(29) Saleem, A.; Patel, M.; Li, X. G.; Gupta, E.; Mendoza, J.; Pantazis, P.; Rubin, E. H. Mechanisms of resistance in a human cell line exposed to sequential topoisomerase poisoning. *Cancer Res.* **1997**, *57*, 5100−5106.

(30) Tamura, H.; Kohchi, C.; Yamada, R.; Ikeda, T.; Koiwai, O.; Patterson, E.; Keene, J. D.; Okada, K.; Kjeldsen, E.; Nishikawa, K. Molecular cloning of a cDNA of a camptothecin-resistant human DNA topoisomerase I and identification of mutation sites. *Nucleic Acids Res.* **1991**, *19*, 69−75.

(31) Kubota, N.; Kanzawa, F.; Nishio, K.; Takeda, Y.; Ohmori, T.; Fujiwara, Y.; Terashima, Y.; Saijo, N. Detection of topoisomerase I gene point mutation in CPT-11 resistant lung cancer cell line. *Biochem. Biophys. Res. Commun.* **1992**, *188*, 571−577.

(32) Fujimori, A.; Harker, W. G.; Kohlhagen, G.; Hoki, Y.; Pommier, Y. Mutation at the catalytic site of topoisomerase I in CEM/C2, a human leukemia cell line resistant to camptothecin. *Cancer Res.* **1995**, *55*, 1339−1346.

(33) Fiorani, P.; Bruselles, A.; Falconi, M.; Chillemi, G.; Desideri, A.; Benedetti, P. Single mutation in the linker domain confers protein flexibility and camptothecin resistance to human topoisomerase I. *J. Biol. Chem.* **2003**, *278*, 43268−43275.

(34) Fertala, J.; Vance, J. R.; Pourquier, P.; Pommier, Y.; Bjornsti, M. A. Substitutions of Asn-726 in the active site of yeast DNA

topoisomerase I define novel mechanisms of stabilizing the covalent enzyme-DNA intermediate. *J. Biol. Chem.* **2000**, *275*, 15246−15253.
(35) Pourquier, P.; Pommier, Y. Topoisomerase I-mediated DNA damage. *Advances Cancer Res.* **2001**, *80*, 189−216.
(36) Stewart, L.; Redinbo, M. R.; Qiu, X.; Hol, W. G. J.; Champoux, J. J. A model for the mechanism of human topoisomerase I. *Science* **1998**, *279*, 1534−1541.
(37) Staker, B. L.; Hjerrild, K.; Feese, M. D.; Behnke, C. A.; Burgin, A. B., Jr.; Stewart, L. The mechanism of topoisomerase I poisoning by a camptothecin analog. *Proc. Natl. Acad. Sci. U.S.A.* **2002**, *99*, 15387−15392.
(38) Chrencik, J. E.; Staker, B. L.; Burgin, A. B.; Pourquier, P.; Pommier, Y.; Stewart, L.; Redinbo, M. R. Mechanisms of camptothecin resistance by human topoisomerase I mutations. *J. Mol. Biol.* **2004**, *339*, 773−784.
(39) Chillemi, G.; D'Annessa, I.; Fiorani, P.; Losasso, C.; Benedetti, P.; Desideri, A. Thr729 in human topoisomerase I modulates anticancer drug resistance by altering protein domain communications as suggested by molecular dynamics simulations. *Nucleic Acids Res.* **2008**, *36*, 5645−5651.
(40) Bayly, C. I.; Cieplak, P.; Cornell, W.; Kollman, P. A. A well-behaved electrostatic potential based method using charge restraints for deriving atomic charges: the RESP model. *J. Phys. Chem.* **1993**, *97*, 10269−10280.
(41) Berman, H. M.; Westbrook, J.; Feng, Z.; Gilliland, G.; Bhat, T.; Weissig, H.; Shindyalov, I. N.; Bourne, P. E. The protein data bank. *Nucleic Acids Res.* **2000**, *28*, 235−242.
(42) *Discovery Studio 2.5 Guide*; Accelrys, Inc.: San Diego, 2009. http://www.accelrys.com (accessed April 1, 2013).
(43) Frisch, M. J.; Trucks, G.; Schlegel, H.; Scuseria, G.; Robb, M.; Cheeseman, J.; Scalmani, G.; Barone, V.; Mennucci, B.; Petersson, G. *Gaussian 09*; Gaussian. Inc., Wallingford, CT, 2009.
(44) Case, D. A.; Cheatham, T. E.; Darden, T.; Gohlke, H.; Luo, R.; Merz, K. M.; Onufriev, A.; Simmerling, C.; Wang, B.; Woods, R. J. The Amber biomolecular simulation programs. *J. Comput. Chem.* **2005**, *26*, 1668−1688.
(45) Wang, J.; Wolf, R. M.; Caldwell, J. W.; Kollman, P. A.; Case, D. A. Development and testing of a general amber force field. *J. Comput. Chem.* **2004**, *25*, 1157−1174.
(46) Hornak, V.; Abel, R.; Okur, A.; Strockbine, B.; Roitberg, A.; Simmerling, C. Comparison of multiple Amber force fields and development of improved protein backbone parameters. *Proteins: Struct., Funct., Bioinf.* **2006**, *65*, 712−725.
(47) Darden, T.; York, D.; Pedersen, L. Particle mesh Ewald: An N·log (N) method for Ewald sums in large system. *J. Chem. Phys.* **1993**, *98*, 10089.
(48) Phillips, J. C.; Braun, R.; Wang, W.; Gumbart, J.; Tajkhorshid, E.; Villa, E.; Chipot, C.; Skeel, R. D.; Kale, L.; Schulten, K. Scalable molecular dynamics with NAMD. *J. Comput. Chem.* **2005**, *26*, 1781−1802.
(49) Petřek, M.; Otyepka, M.; Banáš, P.; Košinová, P.; Koča, J.; Damborský, J. CAVER: A new tool to explore routes from protein clefts, pockets and cavities. *BMC Bioinf.* **2006**, *7*, 316.
(50) Xu, L.; Li, Y.; Zhou, S.; Hou, T. Understanding microscopic binding of macrophage migration inhibitory factor with phenolic hydrazones by molecular docking, molecular dynamics simulations and free energy calculations. *Mol. BioSyst.* **2012**.
(51) Zhang, J.; Hou, T.; Wang, W.; Liu, J. S. Detecting and understanding combinatorial mutation patterns responsible for HIV drug resistance. *Proc. Natl. Acad. Sci. U.S.A.* **2010**, *107*, 1321−1326.
(52) Yang, Y.; Qin, J.; Liu, H. X.; Yao, X. J. Molecular dynamics simulation, free energy calcuiation and structure-based 3D-QSAR studies of B-RAF kinase inhibitors. *J. Chem. Inf. Model.* **2011**, *51*, 680−692.
(53) Xue, W. W.; Qi, J.; Yang, Y.; Jin, X. J.; Liu, H. X.; Yao, X. J. Understanding the effect of drug-resistant mutations of HIV-1 intasome on raltegravir action through molecular modeling study. *Mol. Biosyst.* **2012**, *8*, 2135−2144.
(54) Xue, W. W.; Pan, D. B.; Yang, Y.; Liu, H. X.; Yao, X. J. Molecular modeling study on the resistance mechanism of HCV NS3/4A serine protease mutants R155K, A156V and D168A to TMC435. *Antiviral Res.* **2012**, *93*, 126−137.
(55) Liu, H.; Yao, X.; Wang, C.; Han, J. In silico identification of the potential drug resistance sites over 2009 influenza A (H1N1) virus neuraminidase. *Mol. Pharmaceut.* **2010**, *7*, 894−904.
(56) Kuhn, B.; Kollman, P. A. Binding of a diverse set of ligands to avidin and streptavidin: An accurate quantitative prediction of their relative affinities by a combination of molecular mechanics and continuum solvent models. *J. Med. Chem.* **2000**, *43*, 3786−3791.
(57) Kuhn, B.; Gerber, P.; Schulz-Gasch, T.; Stahl, M. Validation and use of the MM-PBSA approach for drug discovery. *J. Med. Chem.* **2005**, *48*, 4040−4048.
(58) Huo, S.; Massova, I.; Kollman, P. A. Computational alanine scanning of the 1:1 human growth hormone−receptor complex. *J. Comput. Chem.* **2002**, *23*, 15−27.
(59) Hou, T. J.; Zhu, L. L.; Chen, L. R.; Xu, X. J. Mapping the binding site of a large set of quinazoline type EGF-R inhibitors using molecular field analyses and molecular docking studies. *J Chem Inf Comp Sci* **2003**, *43*, 273−287.
(60) Hou, T. J.; Xu, Z.; Zhang, W.; McLaughlin, W. A.; Case, D. A.; Xu, Y.; Wang, W. Characterization of domain−peptide interaction interface. *Mol. Cell. Proteomics* **2009**, *8*, 639−649.
(61) Hou, T. J.; Wang, J.; Li, Y. Y.; Wang, W. Assessing the performance of the molecular mechanics/Poisson Boltzmann surface area and molecular mechanics/generalized Born surface area methods. II. The accuracy of ranking poses generated from docking. *J. Comput. Chem.* **2011**, *32*, 866−877.
(62) Hou, T. J.; Li, Y. Y.; Wang, W. Prediction of peptides binding to the PKA RII alpha subunit using a hierarchical strategy. *Bioinformatics* **2011**, *27*, 1814−1821.
(63) Hou, T.; Zhang, W.; Case, D. A.; Wang, W. Characterization of domain−peptide interaction interface: A case study on the amphiphysin-1 SH3 domain. *J. Mol. Biol.* **2008**, *376*, 1201−1214.
(64) Hou, T.; Wang, J.; Li, Y.; Wang, W. Assessing the performance of the MM/PBSA and MM/GBSA methods. 1. The accuracy of binding free energy calculations based on molecular dynamics simulations. *J. Chem. Inf. Model.* **2011**, *51*, 69−82.
(65) Hou, T.; McLaughlin, W. A.; Wang, W. Evaluating the potency of HIV-1 protease drugs to combat resistance. *Proteins: Struct., Funct., Bioinf.* **2008**, *71*, 1163−1174.
(66) Hou, T.; Li, N.; Li, Y.; Wang, W. Characterization of domain−peptide interaction interface: Prediction of SH3 domain-mediated protein−protein interaction network in yeast by generic structure-based models. *J. Proteome Res.* **2012**, *11*, 2982.
(67) Gohlke, H.; Kiel, C.; Case, D. A. Insights into protein−protein binding by binding free energy calculation and free energy decomposition for the Ras-Raf and Ras-RalGDS complexes. *J. Mol. Biol.* **2003**, *330*, 891−913.
(68) Li, L.; Li, Y.; Zhang, L.; Hou, T. Theoretical studies on the susceptibility of oseltamivir against variants of 2009 A/H1N1 influenza neuraminidase. *J. Chem. Inf. Model.* **2012**, *52*, 2715−2729.
(69) Onufriev, A.; Bashford, D.; David, A. Modification of the generalized Born model suitable for macromolecules. *J. Phys. Chem.* **2000**, *104*, 3712−3720.
(70) Weiser, J.; Shenkin, P. S.; Still, W. C. Approximate atomic surfaces from linear combinations of pairwise overlaps (LCPO). *J. Comput. Chem.* **1999**, *20*, 217−230.
(71) Mai, B. K.; Li, M. S. Neuraminidase inhibitor R-125489−A promising drug for treating influenza virus: Steered molecular dynamics approach. *Biochem. Biophys. Res. Commun.* **2011**, *410*, 688−691.
(72) Mai, B. K.; Viet, M. H.; Li, M. S. Top leads for swine influenza A/H1N1 virus revealed by steered molecular dynamics approach. *J. Chem. Inf. Model.* **2010**, *50*, 2236−2247.
(73) Niu, C.; Xu, Y.; Luo, X.; Duan, W.; Silman, I.; Sussman, J. L.; Zhu, W.; Chen, K.; Shen, J. Dynamic mechanism of E2020 binding to

acetylcholinesterase: A steered molecular dynamics simulation. *J. Phys. Chem. B* **2005**, *109*, 23730−23738.